AIMS Materials Science, 6(5): 833–851.
DOI: 10.3934/matersci.2019.5.833
Received: 11 May 2019
Accepted: 06 September 2019
Published: 17 September 2019

http://www.aimspress.com/journal/Materials

Research article

The cumulative detrimental impact of pressure and autofrettage on the fatigue life of an externally cracked modern tank gun barrel

Mordechai Perl* and Tomer Saley

Aaron Fish Professor Emeritus of Mechanical Engineering-Fracture Mechanics and graduate student respectively. Department of Mechanical Engineering, Ben-Gurion University of the Negev, Beer-Sheva, 84105, Israel

* **Correspondence:** Email: merpr01@bgu.ac.il; Tel: +972086477087.

Abstract: The fatigue life of an externally cracked modern tank gun barrel is controlled by the prevailing combined stress intensity factor (SIF) K_{IN}, which consists of two components: K_{IP}—the SIF caused by internal pressure; K_{IA}—the positive SIF due to the tensile residual stresses induced by autofrettage. K_{IA} values for a single external radial semi-elliptical crack originating at the outer surface of an autofrettaged gun barrel were calculated for a large number of crack configurations by Perl and Saley. In order to assess the combined effect of overstraining and the pressurizing of the barrel during firing, values of K_{IP}, the SIF caused by internal pressure, and those of K_{IN}, the combined SIF, are evaluated. The 3D analysis is performed using the finite element method (FEM) employing singular elements along the crack front. The novel realistic overstrain residual stress fields, incorporating the Bauschinger effect, for the three types of autofrettage, Swage, Hydraulic and Hill's, previously developed, are applied to the barrel. The RSFs are simulated in the finit element (FE) analysis using equivalent temperature fields. Values of K_{IP} and K_{IN} are evaluated for a typical barrel of radii ratio R_0/R_i = 2, crack depths (a/t = 0.005–0.1), crack ellipticities (a/c = 0.2–1.0), and five levels of the three types of autofrettage, (ε = 40%, 60%, 70%, 80%, and 100%). A detailed analysis of the effect of the above parameters on the prevailing SIF is conducted. All three types of autofrettage are found to have a detrimental effect on the barrel's fatigue life. However, the magnitude of life reduction is autofrettage-type dependent. In the case of external cracking, Hydraulic autofrettage is found to be somewhat superior to Swage autofrettage, and Hill's autofrettage is found to be non-realistic. Finally, the results accentuate the importance of the three

dimensional analysis and the incorporation of the Bauschinger effect.

Keywords: external crack; internal crack; gun barrel; autofrettage

A: Crack depth; A_p: Paris' constant; c: Crack half length; E: Young's modulus; K_{00}: Normalizing SIF (Eq 1); K_I: Mode I SIF; K_{IA}: Mode I SIF due to autofrettage; K_{IN}: Combined SIF; K_{INmax}: Maximum combined SIF; K_{IP}: Mode I SIF due to internal pressure; $K_{IP,avg}$: Average SIF along the crack front due to internal pressure; L: Cylinder's half length; n_p: Paris' constant; N: Number of fatigue cycles; N_f: Number of fatigue cycles to failure; P: Internal pressure; R_i: Inner radius of the barrel; R_o: Outer radius of the barrel; r, θ, z: Cylindrical coordinates; t: Barrel's wall thickness; $\Delta\phi$: Parametric angle interval; ε: Level of autofrettage; ν: Poisson's ratio; ξ: Intensity of the adverse effect of autofrettage on external cracks; $\sigma_{\theta\theta}$: Hoop stress component; σ_y : Initial yield stress; ϕ: Parametric angle (Figure 1b); χ: Crack growth rate ratio; Hill: Hill's autofrettage; Hyd: Hydraulic autofrettage; Swage: Swage autofrettage; DEM: Displacement extrapolation method; DOF: Degrees of freedom; FE: Finite element; FEM: Finite element method; LEFM: Linear elastic fracture mechanics; MBT: Main battle tank; RSF: Residual stress field; SIF: Stress intensity factor.

1. Introduction

In order to attain maximal firing range and armor penetrability, modern main battle tanks (MBTs) gun barrels are subjected to very high chamber pressure, severe temperature gradients, and a harsh corrosive environment. In order to acquire these capabilities, modern gun barrels are autofrettaged. Overstraining on the one hand enhances the internal pressure the gun can withstand and reduces its susceptibility to internal cracking at the bore. But on the other hand, autofrettage has an inherent detrimental effect resulting from the tensile hoop stress it induces at the outer part of the gun's wall, which increases sensitivity to external cracking. Gun barrels are overstrained by one of two processes: Hydraulic autofrettage and Swage autofrettage both of which bear these intrinsic advantageous and adverse effects.

The design of the barrel might introduce to its outer surface functional geometrical discontinuities such as keyseats, grooves, part-through holes, etc. Furthermore, as a result of operational field conditions, the outer surface of the barrel might get scratched. During firing, the exterior of the barrel is subjected to repeated action of high pressure loads, and simultaneously it is exposed to corrosive materials and an aggressive environment. The presence of stress concentrators, the repeated loading, and the corrosive environment, may result in initiating a semi-elliptical radial crack growing from the barrel's external surface into the barrel's wall. This fatigue crack might become critical causing catastrophic failure of the barrel at a certain point [1].

Fatigue crack growth rate of such an external crack is controlled by the prevailing combined stress intensity factor (SIF) K_{IN}, which consists of two components: K_{IP}—the SIF caused by internal pressure; K_{IA}—the positive SIF due to the tensile residual stresses induced by autofrettage. The

combined SIF $K_{IN} = K_{IP} + K_{IA}$ depends on both the internal pressure in the barrel as well as on the residual hoop stress induced by autofrettage.

Recently, Perl and Saley [2] evaluated, for the first time, K_{IA} distributions along the front of a single external crack resulting from the three types of autofrettage: Swage, Hydraulic, and Hill's. These distributions were calculated for a large number of crack configurations. In order to enable the evaluation of the barrel's fatigue life due to external cracking, K_{IN} needs to be calculated. Therefore, the purpose of the present analysis to evaluate K_{IN} values based on adequate K_{IP} values, for a single external crack prevailing in an autofrettaged modern gun barrel. This is done by applying a novel, realistic, and experimentally based autofrettage model presented in [1]. This model enables a very accurate replication of both Hydraulic and Swage autofrettage RSFs in a fully or partially overstrained barrel. For comparison reasons, Hill's [3] RSF is also applied. SIFs for a typical smooth gun barrel of radii ratio $R_0/R_i = 2$, for a wide range of crack depth to wall-thickness ratios (a/t = 0.005–0.1), for various crack ellipticities (a/c = 0.2–1.0), and for five levels of autofrettage (ε = 40%, 60%, 70%, 80% and 100%) are evaluated.

2. The autofrettage residual stress field and its simulation

In Perl and Saley [2], a detailed description of the novel realistic autofrettage suggested by Perl and Perry [4] is presented. This model, which is totally based on the experimentally measured stress-strain curve under repeated reversed loading, accurately describes the material behavior including the Bauschinger effect in both tension and compression. The results of this new model applied to a gun made of a typical Cr–Ni–Mo–V barrel-steel (a modified AISI 4340) are presented in Figure 1 of [2] together with Hill's solution. Figure 1 in [2] represent the distribution of the hoop residual stress component, $\sigma_{\theta\theta}^{Res}$, for Hydraulic, Swage and Hill's autofrettage, and for a partially or fully (ε = 40%, 70%, and 100%) overstrained barrel. The same exact results are herein used in the determination of the combined SIF K_{IN}. The residual stress fields of all three types of autofrettage are embodied in the FE analysis using an equivalent temperature field emulating it very accurately. The discrete values of the equivalent temperature field are calculated using the general algorithm developed by Perl [5]. A detailed description of obtaining the equivalent temperature field and its incorporation in the FE analysis is given in Perl [5].

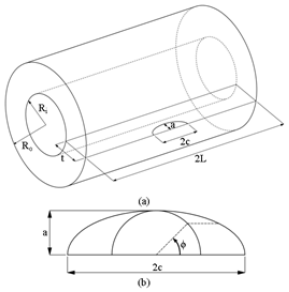

Figure 1. (a) The cylinder with one external crack, and (b) The parametric angle ϕ defining the points on the crack front [2].

3. Three dimensional analysis

As in [2], the three dimensional analysis of the cracked barrel is based on linear elastic fracture mechanics (LEFM). The tube is modeled as an elastic cylinder of inner radius R_i, outer radius R_0, and wall thickness t ($R_0/R_i = 2$, and $t = R_i$) and length $2L$. The cylinder contains an external, radial, semi-elliptical crack of length $2c$ and depth a. The cylinder containing one crack is presented in Figure 1a. In order to avoid end effects, the ratio of the cylinder length to its inner radius L/R_i is taken at least as 4.

The barrel is assumed to be made of a typical Cr–Ni–Mo–V barrel steel (a modified AISI 4340) with an initial yield stress of σ_y = 1050 MPa, Young modulus E = 203 GPa and Poisson's ratio ν = 0.3. As a modern tank gun is considered, the internal pressure is set to be p = 608 MPa. The SIFs K_{IP} and K_{IN} are calculated by the displacement extrapolation (DEM) and the J-integral methods, the same two methods used to calculate K_{IA} in [2]. In the case of very shallow cracks of a/t = 0.005, SIFs are calculated along the crack front at intervals of $\Delta\phi = 3.6°$ for cracks of $a/c \geq 0.4$, and at intervals of $\Delta\phi = 2.25°$ for cracks of a/c = 0.2. For deeper cracks ($a/t \geq 0.01$), SIFs are calculated along the crack front at intervals of $\Delta\phi = 1.8°$ for cracks of $a/c \geq 0.4$, and at intervals of $\Delta\phi = 1.125°$ for cracks of a/c = 0.2.

4. The finite element model

Only a quarter of the cylinder must be analyzed due to the various symmetries of the geometrical configuration (see Figure 2a). A toroidal shape volume consisting of four layers of 20-node isoparametric brick elements is meshed along the entire crack front (see Figure 2). In the first layer, the brick elements are collapsed to wedges forming singular elements [6], to accommodate the singular stress field in the vicinity of the crack front. On top of this layer, three additional layers of 20-node isoparametric brick elements are meshed. The rest of the model is meshed with 10-node tetrahedron elements. In order to maintain high accuracy, the elements near the crack front are chosen to be small, and their size is gradually increased when moving away from it (see Figure 2). The numerical model is solved using the commercial ANSYS 13.0 FE code [7]. The autofrettage residual stress field is incorporated in the FE analysis using an equivalent temperature field, as previously explained. Stress intensity factors are extracted from the FE results employing two methods built into ANSYS: the J-integral [8], and the crack-face displacement extrapolation method. SIFs are calculated at discrete points equally spaced along the crack front, identical to those employed in [2]. In order to maintain the same high accuracy attained for K_{IA} [2] in calculating K_{IP} and K_{IN}, the same FE model is used with an identical element breakdown for each of the crack configurations solved.

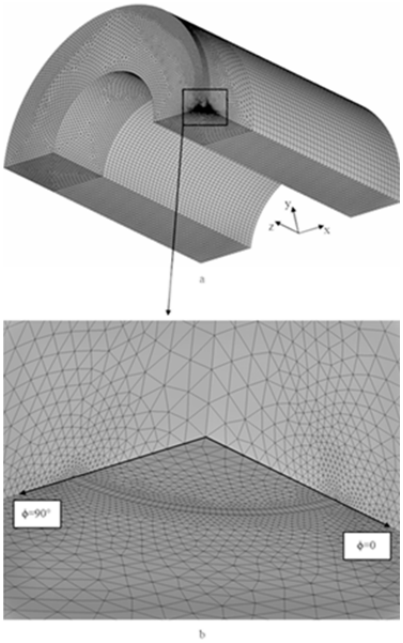

Figure 2. Typical element breakdown for a quarter of a cylindrical pressure vessel with one external crack: (a) the finite element model (b) element breakdown near the crack front

4.1 Validation of the FE model

In [2], the model was thoroughly validated. K_{IP} values obtained by the present model were compared to values obtained by API-579-1 [9], using the weight function method. The present values were found to be within less than 1% of the AIP-579-1 values (see Figure 5 of reference [2]), except for the inner surface point where they differ by about 4%. Furthermore, convergence tests were conducted in order to determine the number of degrees of freedom (DOF) necessary to obtain high accuracy. Those tests show that above 1200000 DOF the error in the SIF is less than about 0.02%. Thus, in order to ensure the same accuracy for K_{IP} and K_{IN} as obtained for K_{IA} in [2], 1600000 DOF are herein employed in all cases. All K_{IP} values obtained in the present analysis are based on exactly the same mesh as the one used for K_{IA} in [2], the same number of DOF, and are evaluated twice employing two independent methods: the J-integral and the DEM procedures.

5. Results and discussion

Values of K_{IP}—the SIF caused by internal pressure and the combined SIF $K_{IN} = K_{IP} + K_{IA}$ are evaluated for a single external radial crack prevailing in a typical barrel of radii ratio $R_0/R_i = 2$, a wide range of relevant crack depth to wall-thickness ratios a/t = 0.005, 0.01, 0.04, 0.07, and 0.1, various crack ellipticities a/c = 0.2, 0.4, 0.6, 0.8, and 1.0, and five levels of Swage, Hydraulic and Hill's autofrettage ε = 40%, 60%, 70%, 80%, and 100%. In total, 375 different 3D external crack cases are analyzed. The values of K_{IA} needed for the evaluation on K_{IN} are imported from [2].

In order to obtain the value of the combined SIF K_{IN}, it is necessary to superimpose the values of K_{IP} on K_{IA}. Thus, their values need to be normalized with respect to the same normalizing SIF which is chosen to be

$$K_{00} = p\sqrt{R_i} \tag{1}$$

5.1. The distribution of K_{IP} the SIF due to internal pressure

K_{IP} distributions along the crack front are presented separately for semi-circular cracks $a/c = 1.0$ and for semi-elliptical ones $a/c < 1.0$.

5.1.1. Semi-circular cracks $a/c = 1.0$

Figures 3 and 4 represent K_{IP}/K_{00} distributions along the crack fronts of two semi-circular external cracks of depths $a/t = 0.005$ and $a/t = 0.1$ respectively. It is important to note that while in the case of an internal crack K_{IP} results from the cumulative effect of both the hoop stress $\sigma_{\theta\theta}$ and the internal pressure p that fully penetrates the crack cavity, in the case of an external crack K_{IP} results only from the prevailing hoop stress in the barrel's wall. The pattern in Figures 3 and 4 are qualitatively similar to those of their internal cracks counterparts [10]. However, in the case of external cracks, K_{IP}/K_{00} maximum occurs near the barrel's outer surface ($\phi = 0°$) and its value decreases monotonically towards the crack deepest points ($\phi = 90°$). As previously noted, internal cracks unlike external cracks, are affected by the penetration of the internal pressure p into the crack's cavity. Thus, for a shallow crack, for example, $a/t = 0.005$, K_{IPmax} of an internal crack is four times larger than that of the external one.

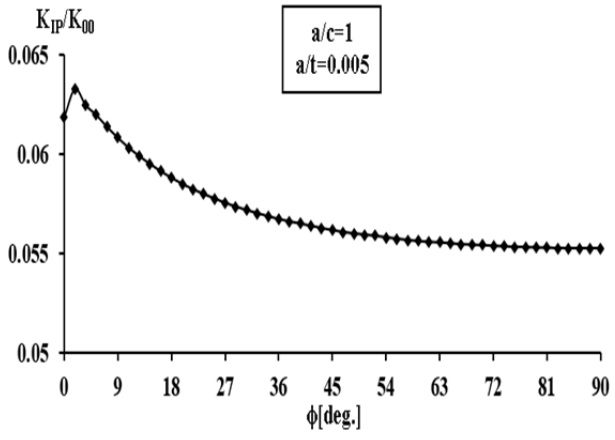

Figure 3. K_{IP}/K_{00} distribution along the front of an external semi-circular crack of depth $a/t = 0.005$ in a barrel of $R_0/R_i = 2$.

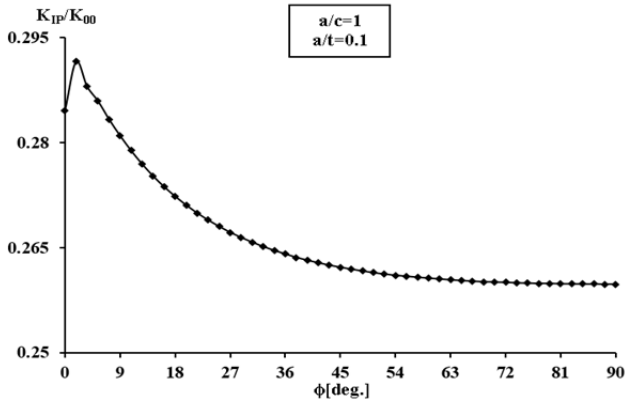

Figure 4. K_{IP}/K_{00} distribution along the front of an external semi-circular crack of depth $a/t = 0.1$ in a barrel of $R_0/R_i = 2$.

5.1.2. Semi-elliptical cracks $a/c < 1.0$

In the case of semi-elliptical cracks, the pattern of K_{IP}/K_{00} distribution along their fronts is ellipticity dependent. Three distinct patterns can be observed:

Cracks of ellipticity $1.0 > a/c > 0.8$

For crack ellipticities larger than $a/c = 0.8$, K_{IP}/K_{00} distribution along the crack front is like that of semi-circular cracks as presented in Figures 3 and 4.

Cracks of ellipticity $0.8 > a/c \geq 0$

Typical K_{IP}/K_{00} distributions along slender semi-elliptical cracks of $a/c = 0.2$ and of depths $a/t = 0.005$ and 0.1 are presented in Figures 5 and 6. In this case, K_{IP}/K_{00} slightly drops from its initial value at the outer surface of the barrel reaching a minimum at $\phi = 4.5°$, and then monotonically increases until reaching its maximum at the deepest point of the crack $\phi = 90°$.

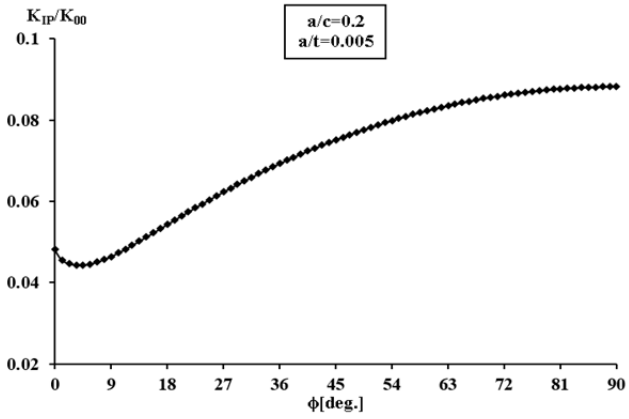

Figure 5. K_{IP}/K_{00} distribution along the front of an external slender semi-elliptical crack, $a/c = 0.2$, of depth $a/t = 0.005$, in a barrel of $R_0/R_i = 2$.

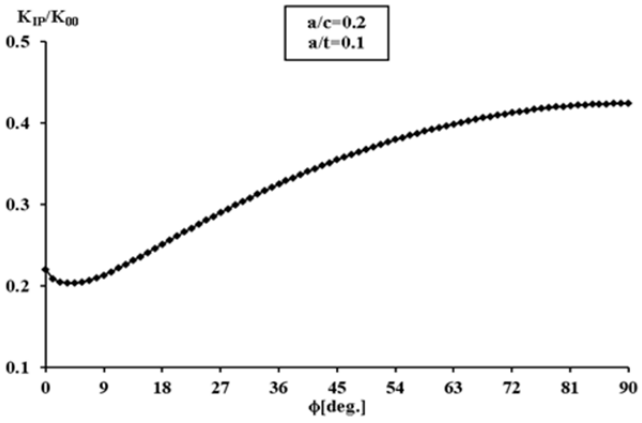

Figure 6. K_{IP}/K_{00} distribution along the front of an external slender semi-elliptical crack, a/c = 0.2, of depth a/t = 0.1, in a barrel of R_0/R_i = 2.

Cracks of ellipticity a/c = 0.8

Cracks of ellipticity a/c = 0.8, such as those presented in Figures 7 and 8, have an almost uniform distribution of K_{IP}/K_{00} along their entire front and are commonly coined as *iso*-K_I cracks. In Figures 7 and 8 the difference between the maximum and the minimum values of K_{IP}/K_{00} is less than 4%, and thus, practically $K_{IPmin}/K_{IPmax} \approx 1$. It is worthwhile noting that there is experimental evidence [11] that no matter what the initial ellipticity of a fatigue crack is, as it grows it tends to reach the ellipticity of $a/c \approx 0.8$.

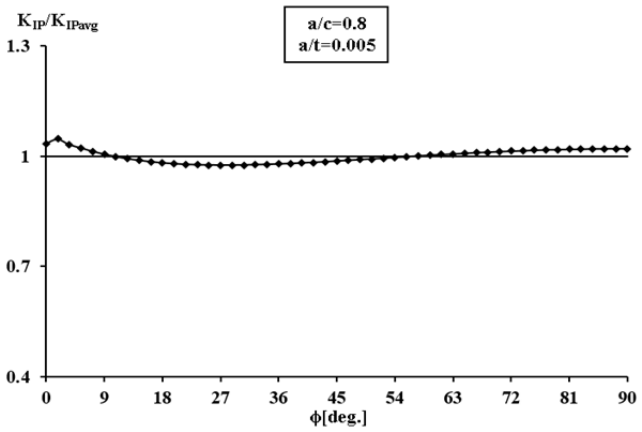

Figure 7. $K_{IP}/K_{IP,avg}$ versus ϕ along the front of an external semi-elliptical *iso*-crack of a/c = 0.8 and depth a/t = 0.005.

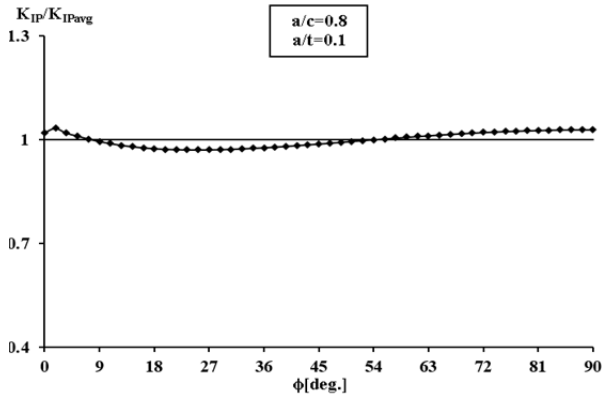

Figure 8. $K_{IP}/K_{IP,avg}$ versus ϕ along the front of an external semi-elliptical *iso*-crack of $a/c = 0.8$ and depth $a/t = 0.1$.

5.2 The distribution of the combined SIF K_{IN} in a fully autofrettaged barrel

The fatigue process is momentarily controlled by the instantaneous prevailing maximal SIF. In the case of a non-autofrettaged barrel, it is K_{IPmax}, the maximal SIF due to internal pressure that controls fracture processes, while in an autofrettaged vessel, fatigue and fracture are controlled by K_{INmax}, the maximal combined SIF, which accounts for both effects: internal pressure and autofrettage.

In order to determine K_{INmax} magnitude and its location along the crack front, one must first superimpose the distributions of K_{IP} and K_{IA} in order to obtain K_{IN} distribution for any particular crack configuration. K_{IP} values were calculated in the present analysis, and K_{IA} values are imported from our previous paper [2]. To enable the superposition K_{IP} and K_{IA} were normalized to the same K_{00}. As the normalizer involves the internal pressure (see Eq 1) and as K_{IA} values depend on the material's properties (see section 3) one should bear in mind that the values of K_{IN}/K_{00} and K_{INmax}/K_{00} that will be presented hereafter, are a special case for the particular material chosen in this analysis, and for an internal pressure of $p = 608$ MPa.

5.2.1. Semi-circular cracks in a fully autofrettaged barrel

Figures 9 and 10 represent the normalized combined SIF K_{IN}/K_{00} distributions along the fronts of two typical semi-circular external cracks of relative depths of $a/t = 0.005$, and 0.1, respectively, prevailing in a fully overstrained barrel by all three types of autofrettage: Hydraulic, Swage and Hill's. All K_{IN}/K_{00} distributions follow a similar pattern: maximum near the outer surface of the barrel, $\phi = 0°$, and then a monotonic decrease towards the crack's deepest point at $\phi = 90°$.

In both cases presented in Figures 9 and 10, K_{INmax}/K_{00} for Swage autofrettage is 4–6% higher than that for Hydraulic autofrettage. Hill's "ideal" autofrettage yields much higher non-realistic K_{INmax}/K_{00} values. To emphasize these results, Table 1 summarizes the relative values for K_{INmax} for various crack depths for the three types of autofrettage.

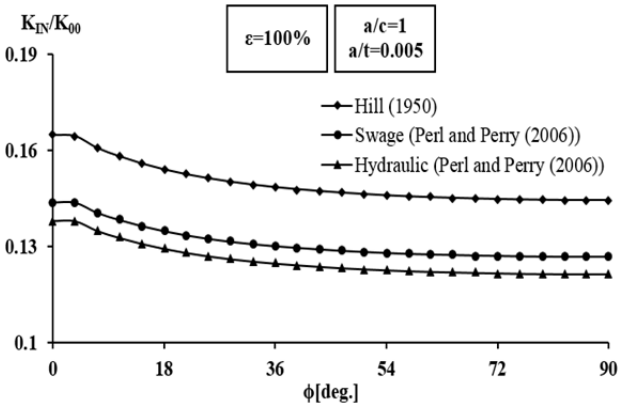

Figure 9. K_{IN}/K_{00} versus ϕ along the front of an external radial semi-circular crack of depth a/t = 0.005, prevailing in a barrel fully overstrained by the three types of autofrettage.

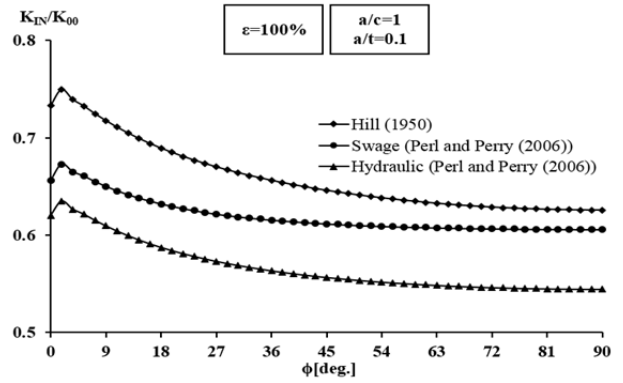

Figure 10. K_{IN}/K_{00} versus ϕ along the front of an external radial semi-circular crack of depth a/t = 0.1, prevailing in a barrel fully overstrained by the three types of autofrettage.

From Table 1 it can be seen that in the case of an externally cracked barrel:

a. The difference between the combined SIF K_{IN} for Swage and Hydraulic autofrettage is between 4% to 6%.
b. The combined SIF K_{IN} for both Swage and Hydraulic autofrettage are lower than Hill's by about 13% to 17%.

Table 1. Relative values of K_{INmax} for full swage hydraulic and Hill's autofrettage for an external semi-circular crack of various depths.

Relative values of K_{INmax} *for* ε = 100%	Relative crack depth				
	a/t = 0.005	a/t = 0/01	a/t = 0.04	a/t = 0.07	a/t = 1.00
$K_{IN\max}^{Swage} / K_{IN\max}^{Hill}$	0.87	0.87	0.88	0.89	0.89
$K_{IN\max}^{Hyd} / K_{IN\max}^{Hill}$	0.83	0.84	0.84	0.84	0.84
$K_{IN\max}^{Swage} / K_{IN\max}^{Hyd}$	1.05	1.04	1.05	1.06	1.06

The typical critical crack length for a modern gun barrel is $(a/t)_{cr} \approx 0.1$, and the combined SIF K_{IN} for Hydraulic and Swage autofrettage is 13% to 17% lower than that of Hill's. Thus, based on Paris' law ($n_p = 2.7$ see [10]), it would mean that crack growth rate for Hydraulic and Swage would be about 60–69% slower than that predict by Hill's, resulting in a higher fatigue life of 65% to 45% relative the one evaluated by Hill's model. Furthermore, based on this data, the fatigue life of an Hydraulically autofrettage barrel would be at least 11% higher than that of a Swaged autofrettage barrel.

5.2.2. Semi-elliptical cracks in a fully autofrettaged barrel

As in the cases of K_{IP}/K_{00} and K_{IA}/K_{00}, the pattern of K_{IN}/K_{00} distribution along the crack front of a semi-elliptical crack depends on the crack's ellipticity. Three distinct groups can be identified:

Cracks of ellipticity $1.0 > a/c > 0.8$

For crack ellipticities larger than $a/c = 0.8$, K_{IN}/K_{00} distributions along the crack front of external cracks is similar to those of semi-circular cracks as presented in Figures 9 and 10, and will not be further discussed herein.

Cracks of ellipticity $0.7 > a/c > 0$

Typical K_{IN}/K_{00} distributions for two slender semi-elliptical cracks ($a/c = 0.2$) of depths $a/t = 0.005$ and 0.1 are presented in Figures 11 and 12. In this cases, K_{IN}/K_{00} slightly drops from its initial value at the outer surface of the barrel reaching a minimum at $\phi = 4.5°$, and then monotonically increases until reaching its maximum at the deepest point of the crack $\phi = 90°$. In Table 2, the relative values for K_{INmax} for slender semi-elliptical cracks ($a/c = 0.2$) of various depths for the three types of autofrettage are presented.

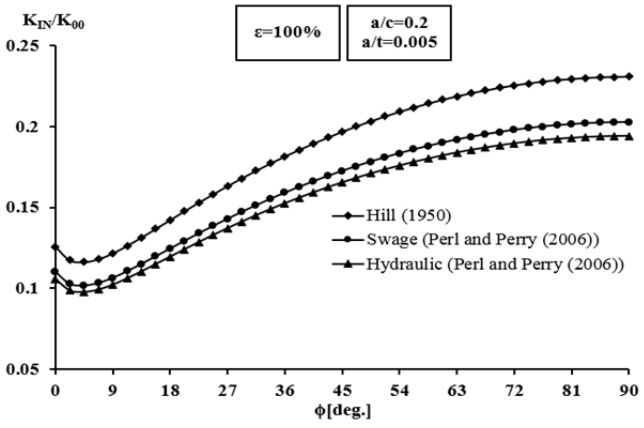

Figure 11. K_{IN}/K_{00} versus ϕ along the front of an external radial slender semi-elliptical crack, $a/c = 0.2$, of depth $a/t = 0.005$, prevailing in a barrel fully overstrained by the three types of autofrettage.

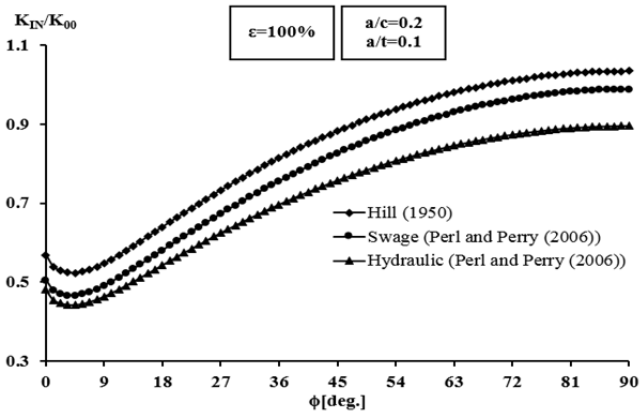

Figure 12. K_{IN}/K_{00} versus ϕ along the front of an external radial slender semi-elliptical crack (a/c = 0.2) of depth a/t = 0.1, prevailing in a barrel fully overstrained by the three types of autofrettage.

Table 2. Relative values of K_{INmax} for full swage hydraulic and Hill's autofrettage for an external slender semi-elliptical crack, a/c = 0.2, of various depths.

Relative values of K_{INmax} for ε = 100%	Relative crack depth				
	a/t = 0.005	a/t = 0/01	a/t = 0.04	a/t = 0.07	a/t = 1.00
$K_{IN\max}^{Swage} / K_{IN\max}^{Hill}$	0.87	0.88	0.90	0.93	0.95
$K_{IN\max}^{Hyd} / K_{IN\max}^{Hill}$	0.84	0.84	0.85	0.85	0.86
$K_{IN\max}^{Swage} / K_{IN\max}^{Hyd}$	1.04	1.05	1.06	1.09	1.10

$K_{IN\max}^{Hyd} / K_{IN\max}^{Hill}$ in this case is practically constant, like in the case of semi-circular cracks. K_{INmax} for hydraulic autofrettage is about 14% to 16% lower than that's of Hill. However, unlike in the case of semi-circular cracks, $K_{IN\max}^{Swage} / K_{IN\max}^{Hill}$ increases with crack depth from 0.87 for the shallowest crack to 0.95 for the deepest one. Consequently, $K_{IN\max}^{Swage} / K_{IN\max}^{Hyd}$ increases with crack depth and therefore, Hydraulic autofrettage would predict a longer fatigue life at least by about 11% than Swage autofrettage for a barrel with an external slender semi-elliptical crack.

Cracks of ellipticity $0.8 \geq a/c \geq 0.7$

This group of cracks exhibits *iso*-K_{IN}/K_{00} distributions as shown in Figures 13 and 14. K_{IN}/K_{00} distributions for Hill's autofrettage are *iso* through the range of ellipticities $0.8 \geq a/c \geq 0.7$. In the cases of Hydraulic and Swage autofrettage *iso*-K_{IN}/K_{00} curves occur for cracks of ellipticity of a/c = 0.8.

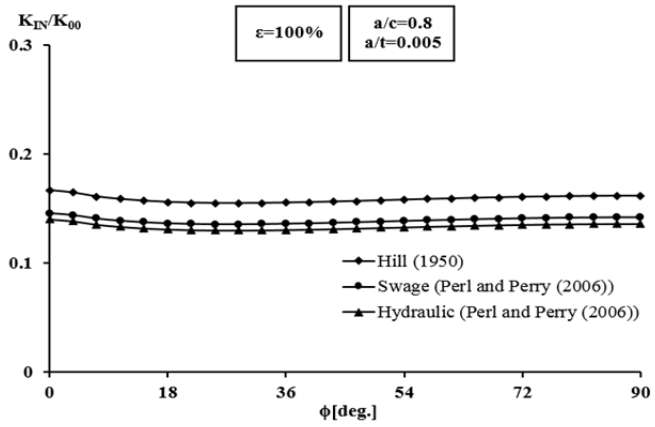

Figure 13. K_{IN}/K_{00} versus ϕ along the front of an external radial slender semi-elliptical crack, a/c = 0.8, of depth a/t = 0.005, prevailing in a barrel fully overstrained by the three types of autofrettage.

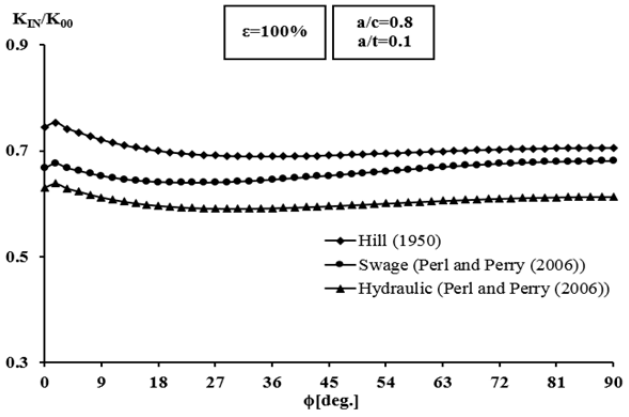

Figure 14. K_{IN}/K_{00} versus ϕ along the front of an external radial slender semi-elliptical crack, a/c = 0.8, of depth a/t = 0.1, prevailing in a barrel fully overstrained by the three types of autofrettage.

5.3 The distribution of the combined SIF K_{IN} in a partially autofrettaged barrel

Figure 15a–c represents K_{IN}/K_{00} for an external radial semi-circular crack of depth a/t = 0.005 prevailing in an overstrained to three different levels of Hill's, swage and hydraulic autofrettage of ε = 100%, 70%, and 40%. Unlike in the case of an internally cracked tube [10], in the case of an externally cracked barrel a reduction in the level of overstraining has a positive effect in reducing the maximum prevailing SIF K_{INmax} for all three types of autofrettage. In the case of an external semi-circular crack of depth a/t = 0.005, Table 3 represents the ratio of the maximum SIF in a fully autofrettaged barrel, K_{INmax} (ε = 100%), to that of a partially autofrettaged tube for Hill's, swage, and hydraulic autofrettage levels of ε = 40%, 60%, and 70%.

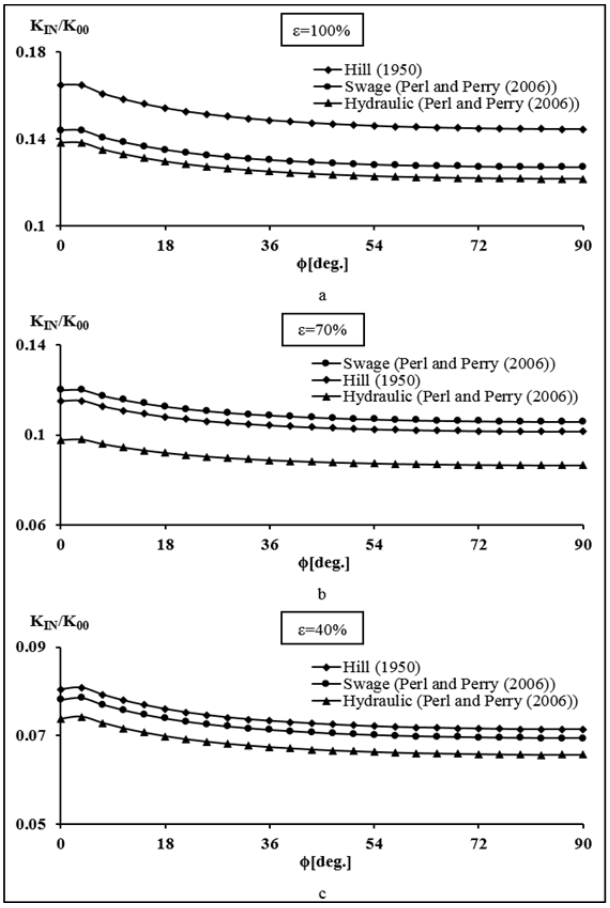

Figure 15. K_{IN}/K_{00} versus ϕ for an external radial semi-circular crack of depth $a/t = 0.005$ prevailing in a cylinder overstrained to three different levels of Hill's, Swage and Hydraulic autofrettage: $\varepsilon = 100\%$, 70% and 40%.

Table 3. Relative K_{INmax} values for an external semi-circular crack of depth $a/t = 0.005$ prevailing in a fully or partially autofrettaged barrel, overstrained to $\varepsilon = 40\%$, 60%, and 70%, by the three types of autofrettage: Hill's, Hydraulic and Swage.

Relative K_{INmax} for various levels of autofrettage	Type of autofrettage		
	Hill	Hydraulic	Swage
K_{INmax} ($\varepsilon = 100\%$)/K_{INmax} ($\varepsilon = 40\%$)	2.00	1.85	1.85
K_{INmax} ($\varepsilon = 100\%$)/K_{INmax} ($\varepsilon = 60\%$)	1.59	1.54	1.33
K_{INmax} ($\varepsilon = 100\%$)/K_{INmax} ($\varepsilon = 70\%$)	1.41	1.39	1.22

As can be anticipated, unlike in the case of an internal crack, in the case of an external one the combined SIF K_{IN}/K_{00} decreases as the level of overstraining decreases for all types of autofrettage. For example, if the level of autofrettage is reduced from $\varepsilon = 100\%$ to $\varepsilon = 70\%$, K_{INmax} decreases by 29%, 28%, and 18% for Hill's, Hydraulic and Swage autofrettage, respectively.

5.4 The intensity of the adverse effect of autofrettage on external cracking

The intensity of the adverse effect of autofrettage on an external crack can be defined as Eq 2:

$$\xi(\%) = \frac{K_{IN\max} - K_{IP\max}}{K_{IP\max}} \cdot 100\% \tag{2}$$

ξ represents the percentage by which K_{IA}, the SIF due to autofrettage, increases the prevailing effective SIF, K_{IN} above and beyond K_{IP}, the SIF due only to internal pressure. The larger ξ, the higher the adverse effect of autofrettage on external cracking of the barrel.

Figure 16a–c exhibits the intensity of the adverse effect of full overstraining (ε = 100%), on external cracks of various depth and ellipticities for the three types of autofrettage. When cracks are shallow $a/t \leq 0.01$, the most substantial region of crack growth, ξ is practically constant and independent of crack depth and ellipticity, and has the values of $\xi \approx 160\%$, 130% and 120% for Hill's, Swage and Hydraulic autofrettage, respectively. As previously stated, the most of the barrel's fatigue life is spent when cracks are very shallow. Crack growth rate in an autofrettaged barrel is given by Paris' Law as:

$$\left(\frac{da}{dn}\right)_{autofrettaged} = A_p (K_{IN\max})^{n_p} \tag{3}$$

and for a non-autofrettaged barrel by:

$$\left(\frac{da}{dn}\right)_{non-autofrettaged} = A_p (K_{IP\max})^{n_p} \tag{4}$$

dividing Eq 3 by Eq 4 and using Eq 2 yields:

$$\chi = \left(\frac{da}{dn}\right)_{autofrettaged} / \left(\frac{da}{dn}\right)_{non-autofrettaged} = (1+\xi)^{n_p} \tag{5}$$

Please note that in Eq 5 ξ is taken as a decimal fraction.

In order to obtain a preliminary estimate of the effect of full autofrettage (ε = 100%) on the total fatigue life of an externally cracked barrel N_f, let's assume for a gun barrel steel n_p = 2.7, and that χ[21], and thus ξ, are practically constant throughout the entire fatigue process for very shallow cracks (see Figure 16). Based on these simplifying assumptions, the following total fatigue life ratios are obtained:

1χ^2 usually changes throughout the fatigue process as it depends on the instantaneous crack ellipticity and depth, the barrel's geometry and its level of autofrettage. In fatigue life calculations, ξ needs to be updated throughout the process.

$$\left(\frac{(N_f)_{non-autofretta\ ged}}{(N_f)_{autofretta\ ged}}\right)_{Swage} = (1+\xi)^{n_p} \approx 9.5 \tag{6}$$

$$\left(\frac{(N_f)_{non-autofretta\ ged}}{(N_f)_{autofretta\ ged}}\right)_{Hyd} = (1+\xi)^{n_p} \approx 8.4 \tag{7}$$

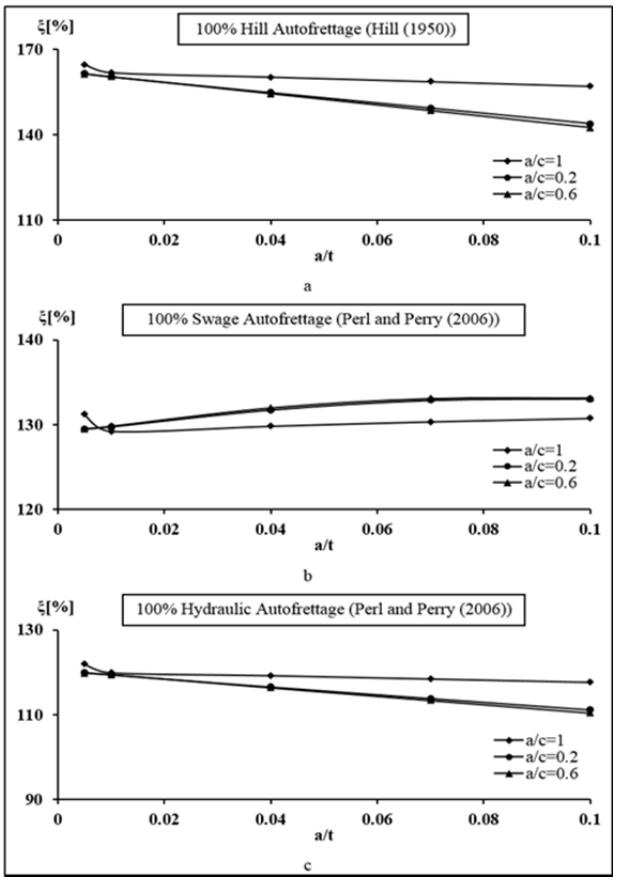

Figure 16. The intensity of the adverse effect of autofrettage on external cracks, ξ, as a function of crack depth in a fully overstrained barrel for various crack ellipticities (a) Hill's, (b) Swage, and (c) Hydraulic autofrettage.

In this case, autofrettage reduces the fatigue life of an externally cracked barrel by a factor of 9.5 and 8.4 for Swage and Hydraulic autofrettage, respectively. These rough results reflect the tremendous detrimental effect autofrettage has on shortening, by almost an order of magnitude, the fatigue life of an externally overstrained cracked barrel as compared to a non autofrettaged tube. Furthermore, it can be seen that in the case of external cracking unlike in the case of internal cracking [10]. Hydraulic autofrettage has a 13% advantage over Swage autofrettage. The high ξ value predicted by Hill's model is definitely non-realistic as it predicts a reduction in the fatigue life by a factor of almost 14.

In the case of deeper cracks, $0.1 \geq a/t \geq 0.01$, while for Hill's and Hydraulic autofrettage, ξ slowly decreases with crack depth in a practically linear manner for Swage autofrettage ξ slightly increases with crack depth. This difference is a direct result of the different residual hoop stress distributions for the three types of autofrettage (see Figure 1 of [2]).

In order to further investigate the intensity of the adverse effect of overstraining on the fatigue life, ξ was evaluated for barrels containing a single external semi-circular crack of depths $0.1 \geq a/t \geq 0.005$ fully or partially overstrained (ε = 100%, 70%, and 40%) by the three types of autofrettage (a) Hill, (b) Swage, and (c) Hydraulic is presented in Figure 17. In this case of a semi-circular external crack, ξ is practically crack-depth independent. As could have been anticipated, as the level of autofrettage is reduced the intensity of its adverse effect on external cracks decreases. For example, when the level of overstraining is reduced from 100% to 70%, ξ decreases by about: 80%, 38%, 65% for Hill's, Swage and Hydraulic autofrettage, respectively.

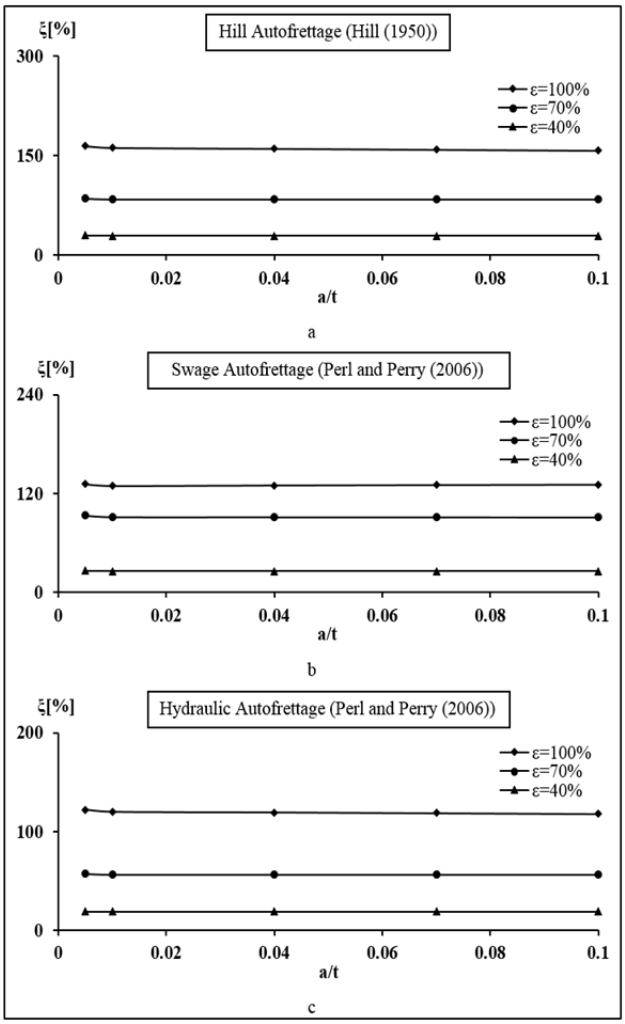

Figure 17. The intensity of the adverse effect of Autofrettage on external cracks, ξ, as a function of crack depth for a single semi-circular crack in a fully or partially overstrained barrel (a) Hill's, (b) Swage and (c) Hydraulic autofrettage.

6. Conclusions

The combined SIF $K_{IN} = K_{IP} + K_{IA}$ for a single external radial 3D crack prevailing in an overstrained smooth gun barrel was evaluated for 375 cases examining the effects of the type and the level of autofrettage, as well as the influence of the crack's geometry. K_{IN} values were evaluated for three types of autofrettage: Swage, Hydraulic and Hill's, for five levels of overstraining ε = 40%, 60%, 70%, 80%, and 100%, for crack depths of a/t = 0.005, 0.01, 0.04, 0.07, and 0.1, and for various crack ellipticities a/c = 0.2, 0.4, 0.6, 0.8, and 1.0. Furthermore, in order to keep uniform accuracy, K_{IP} values for all the above geometrical crack configurations were evaluated using an identical mesh to the one used for the evaluation of the corresponding K_{IA} in [2].

All three types of autofrettage are found to considerably shorten the fatigue life of an externally cracked barrel, as compared to a non-autofrettaged barrel's fatigue life. However, the magnitude of this adverse effect is autofrettage-type dependent. Unlike in the case of internal cracking [2], in the case of external cracking Hydraulic autofrettage is found to be superior to the Swage one predicting a 13% higher barrel's fatigue life, as presented in the case in section 5.4. Hill's "ideal" autofrettage is found to be non-realistic, yielding exaggerated underestimates of the barrel's fatigue life. This is a direct consequence of the fact that Hill's residual stress field (RSF) ignores the Bauschinger effect, which in the case of the realistic Swage and Hydraulic RSF, results in a substantial reduction of the material's yield stress and thus, in lower K_{IN} values.

Reducing the level of autofrettage reduces considerably the intensity of adverse effect of overstraining on external cracks for all types of autofrettage and thus, considerably prolonging the barrel's fatigue life. For example, reducing ε from 100% to 70% results in a decrease of ξ of about 80%, 38%, 65% for Hill's, Swage and Hydraulic autofrettage, respectively.

Conflict of interests

The authors declare no conflict of interests.

References

1. Kapp JA (1985) Predicting catastrophic outside diameter initiated fatigue failure of thick-walled cylinders using low cycle fatigue data. ARLCBTR-85035, Benet Weapons Laboratory, Watervliet.
2. Perl M, Saley T (2019) The detrimental effect of Swage and Hydraulic autofrettage on externally cracked modern gun barrels. *Def Technol* 15 146–153.
3. Hill R (1950) The Mathematical Theory of Plasticity, New York: Oxford University Press.
4. Perl M, Perry J (2006) An experimental-numerical determination of the three dimensional autofrettage residual stress field incorporating bauschinger effect. *J Press Vess-T ASME* 128: 173–178.
5. Perl M (1988) The temperature field for simulating partial autofrettage in an elasto-plastic thick-walled cylinder. *J Press Vess-T ASME* 110: 100–102.

6. Barsom RS (1976) On the use of isoparametric finite elements in linear fracture mechanics. International. *Int J Numer Meth Eng* 10: 25–37.
7. ANSYS Release 13.0 (2010) Available from: https://www.ansys.com/products/structures.
8. Rice JR (1968) A path independent integral and the approximate analysis of strain Concentration by notched and cracks. *J Appl Math* 35: 379–386.
9. API 579-1/ASME FFS-1 Fitness for Service (2007) Available from: gost-snip.su › download › api_5791_asme_ffs1_fitnessforservice.
10. Perl M, Saley T (2017) Swage and hydraulic autofrettage impact on fracture endurance and fatigue life of an internally cracked smooth gun barrel part II—The combined effect of pressure and overstraining. *Eng Fract Mech* 182c: 386–399.
11. Lin XB, Smith RA (1998) Fatigue growth prediction of internal surface cracks in pressure vessels. *J PressVess-T ASME* 120: 17–23.

AIMS Press